Limit Analysis and Conic Programming for Gurson-Type Spheroid Problems

F. Pastor, P. Thoré, D. Kondo, and J. Pastor

Abstract In his famous 1977-paper, Gurson used the kinematic approach of Limit Analysis (LA) about the hollow sphere model with a von Mises solid matrix. The computation led to a macroscopic yield function of the "Porous von Mises"-type materials. Several extensions have been further proposed in the literature, such as those accounting for void shape effects by Gologanu et al. (J. Eng. Mater. Technol. 116:290–297, 1994; Continuum Micromechanics, Springer, Berlin, 1997), among others. To obtain pertinent lower and upper bounds to the exact solutions in terms of LA, we have revisited our existing kinematic and static 3D-FEM codes for spherical cavities to take into account the model with confocal spheroid cavity and boundary. In both cases, the optimized formulations have allowed to obtain an excellent efficiency of the resulting codes. A first comparison with the Gurson criterion does not only show an improvement of the previous results but points out that the real solution to the hollow sphere model problem depends on the third invariant of the stress tensor. A second series of tests is presented for oblate cavities, in order to analyze the above-mentioned works in terms of bound and efficiency.

F. Pastor
Laboratoire de mécanique de Lille (LML), UMR 8107 CNRS, Villeneuve d'Ascq, France
e-mail: franck.pastor@skynet.be

P. Thoré · J. Pastor (✉)
Laboratoire LOCIE, Polytech' Annecy-Chambéry, Université de Savoie, 73376 Le Bourget du Lac, France
e-mail: joseph.pastor@univ-savoie.fr

P. Thoré
e-mail: philippe.thore@orange.fr

D. Kondo
Institut D'Alembert, Université Pierre et Marie Curie, UMR 7190 CNRS, 75252 Paris Cedex 05, France
e-mail: djimedo.kondo@upmc.fr

G. Saxcé et al. (eds.), *Limit State of Materials and Structures*,
DOI 10.1007/978-94-007-5425-6_12,

1 Introduction

As regards the ductile failure of porous materials, the celebrated plasticity criterion of Gurson [8] is based on a micro-macro approach and on limit analysis (LA). Gurson's model treats a hollow von Mises sphere or cylinder with macroscopic strain imposed on its boundary. The computation, performed under uniform strain rate boundary conditions, leads to a macroscopic yield function for the "Porous von Mises"-type materials.

Gurson's analysis consists in the use of the LA kinematic approach in order to obtain an upper bound to the macroscopic criterion of the spherically porous material, at least in the sense of the Composite Sphere Assemblage of Hashin. An efficient parametric refinement of Gurson's model has been proposed in [24] and [25] to define the widely used Gurson-Tvergaard-Needleman (GTN) model. More recently, several extensions of the Gurson model have been proposed, the probably most important developments being those accounting for void-shape effects [4, 7, 14]. Mention can also be made of models taking into account plastic anisotropy [1, 13].

On the other hand, using a finite element discretization of the mechanical systems, both static and kinematic methods of LA have been elaborated to obtain rigorous lower and upper bounds in order to control Gurson's kinematic approaches for cylindrical as well as spherical cavities, first reported in [20]. In [3] and [19], these two LA approaches made it possible to numerically determine the yield criteria of a cylindrically porous material, also proving that the Gurson criterion is approximate, and does not exhibit the corner of the exact criterion on the mean stress axis in plane strain. On the contrary, in the subsequent work [23] the Gurson criterion appears to be satisfactory for materials with spherical cavities, unfortunately without considering the dissymmetry as in the present work.

The main advantage of these LA numerical approaches is that they give rigorous lower and upper bounds to the macroscopic criterion together with their controllability *a posteriori* from the final optimal solution. This capability to control numerical or analytical results is central and was used in [18], and in [22] for example.

In the present paper, we briefly present the extension in [15] of the 3D static and kinematic codes of [23] for von Mises matrices to the spheroid (confocal) cavity case. Then, comparisons with previously mentioned works for spherical and oblate cavites conditions are presented and discussed.

2 The Hollow Spheroid Model

The considered hollow spheroid model is made up of a single spheroidal cavity embedded in a confocal spheroidal cell. The solid matrix is an isotropic, homogeneous, and rigid-plastic von Mises material. Figure 1 presents the geometrical model, where the given aspect ratio a_1/b_1 and porosity f allow to determine the characteristics a_2 and b_2 of the confocal spheroidal boundary. Let us consider the three-dimensional point of view, and denote Σ and E the macroscopic stress and

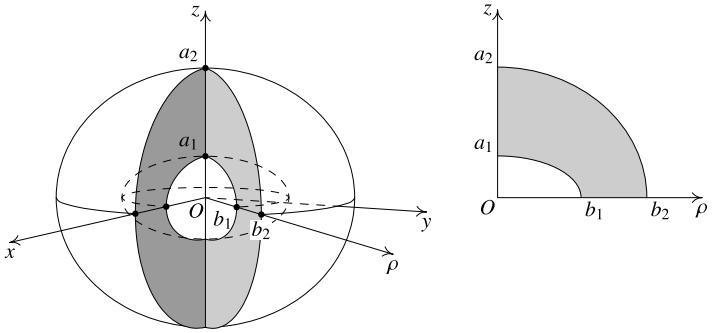

Fig. 1 The hollow spheroid model ($a_1/b_1 = 0.5,\ f = 0.1$)

strain rate tensors. These quantities are classically related to the microscopic fields by their average over the model of volume V:

$$\Sigma_{ij} = \frac{1}{V}\int_V \sigma_{ij}\, dV; \qquad E_{ij} = \frac{1}{2V}\int_{\partial V} (u_i n_j + u_j n_i)\, dS, \tag{1}$$

where ∂V denotes the external boundary of the model, and u the velocity vector.

Under the Hill-Mandel boundary conditions, here $u_i = E_{ij}x_j$ on the external boundary, the overall virtual dissipated power $P_{\text{tot}} = \Sigma_{ij}E_{ij}$ can be written as follows:

$$P_{\text{tot}} = V(\Sigma_{\text{m}}E_{\text{m}} + \Sigma_{\text{ps}}E_{\text{ps}} + \Sigma_{\text{gps}}E_{\text{gps}} + \Sigma_{yz}2E_{yz} + \Sigma_{zx}2E_{zx} + \Sigma_{xy}2E_{xy}), \tag{2}$$

where the macroscopic stresses (the loading parameters in terms of limit analysis) and the associated strain rates are here defined as:

$$\Sigma_{\text{m}} = \frac{1}{3}(\Sigma_x + \Sigma_y + \Sigma_z); \qquad \Sigma_{\text{gps}} = \frac{(\Sigma_x + \Sigma_y)}{2} - \Sigma_z;$$
$$\Sigma_{\text{ps}} = \frac{\sqrt{3}}{2}(\Sigma_x - \Sigma_y); \tag{3}$$

$$\Sigma_{yz}; \quad \Sigma_{zx}; \quad \Sigma_{xy}; \tag{4}$$

$$E_{\text{m}} = (E_x + E_y + E_z); \qquad E_{\text{gps}} = \frac{2}{3}\left(\frac{(E_x + E_y)}{2} - E_z\right);$$
$$E_{\text{ps}} = \frac{1}{\sqrt{3}}(E_x - E_y); \tag{5}$$

$$2E_{yz}; \quad 2E_{zx}; \quad 2E_{xy}. \tag{6}$$

In these definitions the subscripts (*gps* for generalized plane strain, and *ps* for plane strain) were defined in [19], as $\Sigma_{\text{gps}} = 0$ is the usual relation in plane strain for the von Mises material. From the matrix isotropy and the spheroidal geometry

of the model, the resulting material is transversally isotropic around the axis z. Here is investigated the macroscopic criterion $g(\Sigma)$ in the $(Oxyz)$ anisotropy frame.

To compare with Gologanu's axisymmetric results, we search for the projection of $g(\Sigma)$ on the $(\Sigma_{\text{gps}}, \Sigma_{\text{m}})$ plane by optimizing Σ_{gps} for fixed uniform stresses Σ_{m}, the other stress components defined in (4) being free. Then $\frac{\partial g}{\partial \Sigma_{ij}} = 0 = 2E_{ij}$ for $i \neq j$, and $\frac{\partial g}{\partial \Sigma_{\text{ps}}} = 0 = E_{ps}$ since the macroscopic material verifies the normality law. As a final result, loadings can be restricted to the principal macroscopic strain rates E (as well as Σ since $(Oxyz)$ is a transverse-isotropy frame) with $E_{\text{ps}} = 0$.

Moreover, all the axes in the horizontal plane of Fig. 1 are equivalent; therefore, in the above-mentioned projection problem we also impose, although this is not mandatory, $\Sigma_x = \Sigma_y$ as well as $E_x = E_y$ in fact. Indeed, when non imposed *a priori*, these equalities are always verified in the optimal solutions, giving by the way a good control of the mesh quality.

Finally, the overall external power P_{tot} here reduces to:

$$P_{\text{tot}} = V(\Sigma_{\text{m}} E_{\text{m}} + \Sigma_{\text{gps}} E_{\text{gps}}). \tag{7}$$

Therefore, the one-eighth of the hollow spheroid is meshed into tetrahedral elements as shown in Fig. 2. This mesh respects the symmetries of the problem since the vertical coordinate planes are equivalent regarding the distribution of elements, giving rise to a well-conditioned numerical problem. Note that the macroscopic equivalent stress Σ_{eqv} is, in the present case, linked to Σ_{gps} by:

$$\Sigma_{\text{eqv}}^2 = \frac{3}{2}\,\text{dev}(\Sigma) : \text{dev}(\Sigma) = \Sigma_{\text{gps}}^2 = (\Sigma_x - \Sigma_z)^2, \tag{8}$$

where $\text{dev}(\Sigma)$ is the deviatoric part of Σ.

Hereafter, we first briefly present both lower/upper limit analysis approaches which have recently been detailed in [15]. The basis of the development of these numerical tools are their versions presented in [23] for spherical cavities; therefore we only detail here the modifications and improvements implemented for the present case. In a second step, results are analyzed and compared to those provided in [6] and [7] for oblate models under uniform strain rate boundary conditions.

3 Limit Analysis: The Static Method

3.1 The von Mises Criterion

As classically, the criterion is written as:

$$f(\sigma) = \sqrt{J_2} \quad \text{with } J_2 = \frac{1}{2}\text{tr}\left(s^2\right) \quad \text{and} \quad s = \sigma - \frac{1}{3}\text{tr}(\sigma)\delta, \tag{9}$$

where δ is the second order unit tensor.

Then in an (x, y, z) reference frame, the full 3D criterion reads:

$$\sqrt{\left[\frac{2}{\sqrt{3}}\left(\frac{\sigma_x+\sigma_y}{2}-\sigma_z\right)\right]^2+(\sigma_x-\sigma_y)^2+(2\tau_{yz})^2+(2\tau_{zx})^2+(2\tau_{xy})^2}\leq 2k. \tag{10}$$

The constant k is the limit in pure shear, also given by $\sigma_0/\sqrt{3}$ where σ_0 is the tensile strength of the von Mises material. It should be noted that (10) can be written, after obvious changes of variables, as a conic constraint for the conic optimizer MOSEK [12]:

$$\sqrt{\sum_{j=1}^{5} x_j^2}\leq x_6=2k. \tag{11}$$

3.2 Numerical Implementation

For each aspect ratio a_1/b_1, the inner and outer matrix boundaries of the spheroid mesh are adapted from the spherical case to obtain their confocal forms in the final mesh. Each triangle of a polyhedral surface n is the top basis of a prism whose the bottom basis is the corresponding triangle of the surface $n-1$, and so on going to the cavity. Each prism is divided into two tetrahedrons and three pyramids. Each pyramid is also divided into four tetrahedrons. Hence, each prism is meshed using 14 tetrahedral elements. For example the mesh of Fig. 2 involves 4 concentric layers ($nlay = 4$) of 4×4 prisms ($ndiv \times ndiv$, $ndiv = 4$) each, resulting finally in $nlay \times ndiv^2 \times 14 = 896$ tetrahedrons As the model boundaries are not homothetic and the practical number of triangles forming the resulting polyhedral mesh boundaries is not infinite, the resulting mesh porosity does not exactly equal the input porosity. Then, in a first step for each case of porosity and aspect ratio, the distribution of the angle α (see Fig. 2 right) is optimized to precisely retrieve the desired porosity by progressively concentrating this distribution towards the most curved zone. In a final step the radial distribution of the spheroid layers is also optimized to obtain the best value for the isotropic loading ($\Sigma_{\text{gps}} = 0$) with the static code.

The local stress field is chosen as linearly varying in x, y, z in each tetrahedral element, and represented by a 6-component tensor σ for each vertex of this tetrahedral element. Consequently this stress field can be discontinuous across any element boundary, which has been proven to be indispensable in the finite element static approach [17]. Finally, to reduce the size of the constraint matrix of the numerical problem, a change of variables $\sigma \rightarrow (x_0, \ldots, x_5)$ is performed, where $x_0 = \operatorname{tr}\sigma$ and x_1 to x_5 defined in (11), so that only the definition of x_6 is needed as a new constraint (and a new auxiliary variable) for each tetrahedron vertex.

To get a statically admissible microscopic stress field, the definition of the macroscopic stresses and of the selected loading parameters, the equilibrium equations

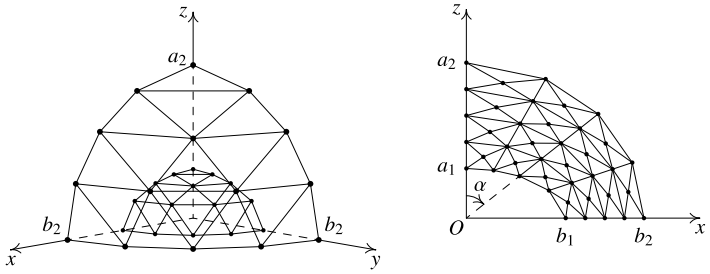

Fig. 2 General view and Oxz plane of a 896-tetrahedron mesh ($a_1/b_1 = 0.5$, $f = 0.1$)

and the stress vector continuity across the inter element triangles, the boundary and symmetry conditions give rise to a final matrix of equality constraints.

To enforce the stress field to be plastically admissible, the criterion (10) is imposed at each apex of the tetrahedron; hence, due to its convexity, the criterion is fulfilled anywhere in the element. For each tetrahedron the four conic inequalities are directly handled by MOSEK by simply indicating the names of the variables x_i involved in the criteria (11). The final numerical problem is a constrained conic programming one, which is a specificity of MOSEK.

Finally, concerning the objective functional to be optimized, Σ_{m} is given successive desired values and Σ_{gps} is minimized; when Σ_{m} is close to its maximum value, then Σ_{gps} is fixed and Σ_{m} is maximized for better convergence of the optimization process.

4 Limit Analysis: The Kinematic Method

4.1 Dissipated powers

Let us recall that, from the virtual power principle, the total dissipated power P_{tot} here reads:

$$\Sigma_{\mathrm{m}} E_{\mathrm{m}} + \Sigma_{\mathrm{gps}} E_{\mathrm{gps}} = (P_{\mathrm{vol}} + P_{\mathrm{disc}})/V = P_{\mathrm{tot}}/V, \tag{12}$$

where the volumic dissipated power $P_{\mathrm{vol}} = \int_{V_{\mathrm{m}}} \pi(d)\, dV$ and $\pi(d)$ is now defined as:

$$\pi(d) = 2k\sqrt{\left(\frac{\sqrt{3}}{2}(d_{xx} + d_{yy})\right)^2 + \left(\frac{1}{2}(d_{xx} - d_{yy})\right)^2 + d_{yz}^2 + d_{zx}^2 + d_{xy}^2}. \tag{13}$$

The power dissipated by the velocity jump $[u]$ on the discontinuities is given by:

$$P_{\mathrm{disc}} = \int_{S_{\mathrm{d}}} \pi\big([u]\big)\, dS = \int_{S_{\mathrm{d}}} k\big|[u_t]\big|\, dS = \int_{S_{\mathrm{d}}} k\sqrt{[u_{t_1}]^2 + [u_{t_2}]^2}\, dS, \tag{14}$$

where S_d is the set of discontinuity surfaces; for each discontinuity surface, $[u_{t_1}]$ and $[u_{t_2}]$ are the tangential displacement velocity jumps in an orthonormal frame (n, t_1, t_2) whose n is normal to this discontinuity surface.

4.2 Numerical Implementation

The above-mentioned mesh type is also used for the kinematic approach. The displacement velocity field is chosen as linearly varying in x, y, z in each tetrahedral element, and any triangular surface common to two contiguous tetrahedrons is a potential surface of velocity discontinuity. Then the variables are (u_x, u_y, u_z) velocity vectors located at the apices of each tetrahedron.

To get a kinematically admissible velocity field, the definition of the selected macroscopic variables E_m, E_gps, E_ps from E_{xx}, E_{yy}, E_{zz}, the incompressibility and symmetry conditions, and the strain rate loading ones (i.e. $u_i = E_{ij} x_j$ on each apex on the boundary triangles) form a final constraint matrix.

Concerning the definition of the functional to be optimized, by taking into account (13), we can upper bound the volumetric dissipated power in the tetrahedron by writing:

$$\pi(d) \leq Y; \qquad P_\mathrm{vol}^\mathrm{el} \leq V^\mathrm{el}\, Y \tag{15}$$

for each tetrahedron whose volume is denoted V^el. The first inequality in (15) gives one conic constraint and one non-negative auxiliary variable Y for each element.

As the velocity jump $[u]$ is linear on each triangular discontinuity side, whose surface is denoted S^side, we use the convexity of $\pi([u])$ to upper bound P_disc by writing at each apex i of the side ($i = 1$ to 3):

$$\pi\big([u]_i\big) \leq Z_i, \tag{16}$$

where the Z_i are new non-negative auxiliary variables, and $P_\mathrm{disc}^\mathrm{side} \leq S^\mathrm{side}\,(Z_1 + Z_2 + Z_3)/3$, resulting in three conic constraints for each discontinuity side. Then, using these definitions and after integrations over the mesh, we substitute the final upper bound $P_\mathrm{tot}^\mathrm{ub}$ for P_tot in the following.

In the present case of two loading parameters, Σ_m and Σ_gps, the following functional is used to define the points of the macroscopic criterion for zero or small absolute values of Σ_gps:

$$\Sigma_\mathrm{m} = \min\big(P_\mathrm{tot}^\mathrm{ub}/V - \Sigma_\mathrm{gps}^0\, E_\mathrm{gps}\big)/E_\mathrm{m}^0, \quad \text{with } E_\mathrm{m}^0 = 1. \tag{17}$$

To obtain other non-zero $(\Sigma_\mathrm{m}^0, \Sigma_\mathrm{gps})$ points, we chose the following functional, for better convergence, as in the static case:

$$\Sigma_\mathrm{gps} = \min\big(P_\mathrm{tot}^\mathrm{ub}/V - \Sigma_\mathrm{m}^0\, E_\mathrm{m}\big)/E_\mathrm{gps}^0, \quad \text{with } E_\mathrm{gps}^0 = \pm 1. \tag{18}$$

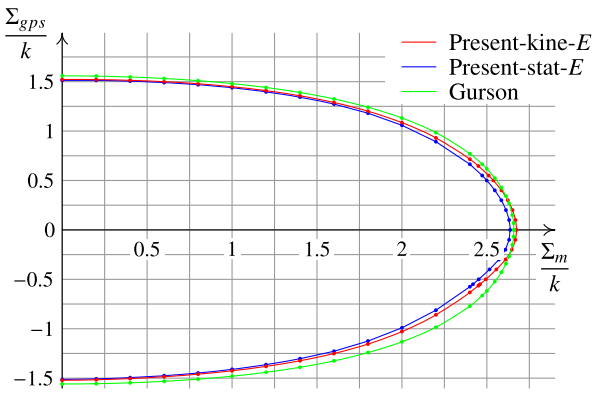

Fig. 3 Comparison with the Gurson criterion ($a_1/b_1 = 1$, $f = 0.1$)

Remark For both static and kinematic methods the final conic problem is solved using MOSEK, and the admissible character of the optimal solution field is checked *a posteriori*.

5 The Tests

Under uniform strain rate on the boundary, in the static case the mesh involves 13 layers of 12×12 prisms (with triangular basis) composed of 14 tetrahedrons, resulting in a conic programming problem handling about 730,000 variables and 658,000 constraints. In the kinematic case the mesh is the same, but with $11 \times 11 \times 11$ prisms resulting in 663,000 variables and 445,000 constraints. CPU times are about 3,000 seconds in the static case and 5,000 seconds in the kinematic one, with the release 5 of MOSEK on a recent Apple Mac Pro (using one core). For uniform stress loading, the figures are similar. In both cases the memory limitation of this release does not allow to consider more refined meshes. These CPU times also explain that obtaining the full numerical yield criterion, (then with meshes not limited to the one-eighth of the spheroid) and for various other geometries, does not seem realistic without defining a specific decomposition of the problem as in [16] and [9], at least for the moment.

Since the von Mises criterion is an even function in terms of stress, we limit the study to nonnegative values of Σ_m. In this section, the loading is axisymmetric for all tests and $\Sigma_{\text{eqv}} = |\Sigma_{\text{gps}}|$. We begin by testing the codes in the spherical cavity case to compare with the Gurson criterion in the whole $\Sigma_m \geq 0$ half plane. Then we analyze the oblate case with a ratio $a_1/b_1 = 0.2$ (see Fig. 1) for the case of uniform strain rate (E) on the boundary to compare the solutions with the analytical results of [6, 7] where the results are given in terms of $\Sigma_z - \Sigma_\rho = -\Sigma_{\text{gps}}$.

Table 1 Comparison of Gurson criterion and present kinematic results for negative Σ_{gps} and $f = 0.3$

Σ_m	-(Gurson Σ_{eqv})	-(3D-kine Σ_{gps})
0.0	1.21244	1.17101
0.2	1.20122	1.15328
0.4	1.16658	1.10820
0.6	1.10521	1.03030
0.8	1.01017	0.91075
1.0	0.86703	0.73865
1.2	0.63821	0.49854
1.26587	0.52497	0.4
1.32245	0.39332	0.3
1.36344	0.24993	0.2
1.38674	0.09075	0.1
1.39023	0.0	0.07634
1.39432	–	0.0

5.1 Spherical Cavity, Uniform Strain Rate Loading

The celebrated Gurson criterion reads:

$$\frac{\Sigma_{\text{eqv}}^2}{3k^2} + 2f\cosh\left(\frac{\sqrt{3}\Sigma_m}{2k}\right) = 1 + f^2. \tag{19}$$

Figure 3 gives the lower bounds (green color) and upper bounds (red color) together with the graph of Gurson's criterion. The numerical bounds are very close to each other and the Gurson graph is always beyond the kinematical approach, except at the vicinity of the Σ_{m} axis, as expected from the exact nature of the solution of Gurson on this axis.

More surprisingly, it can be seen that the real criterion is not really symmetric with respect to the horizontal axis; this means (from (8)) that, even for spherical cavities, the criterion depends on the third invariant of the macroscopic stress; this feature has been observed by Danas et al. [2] using a non linear homogenization method and recently confirmed in [21]. Up to our knowledge a possible small influence of the third stress invariant for "porous von Mises" materials was first noted in [5], through an only kinematic numerical approach based on some of the *continuous* velocity fields of Lee and Mear [11].

It can also be concluded that using the Gurson criterion in the usual ($\Sigma_{\text{eqv}} = |\Sigma_{\text{gps}}|, \Sigma_{\text{m}}$) frame is not pertinent; indeed, for a porosity of 0.3 (usual value in geotechnics and polymers) the results of Table 1 show that the difference between Gurson's values and our present 3D-kinematic results for negative Σ_{gps} becomes really significant.

Remark For $\Sigma_m = 0$ and $f = 0.1$, the Hashin-Strikmann (H-S) upper bound given by Willis and others (see [10]) (here $1.5093 = \sqrt{3}(1-f)/\sqrt{1+2f/3}$), is lower

Table 2 Comparison of Gurson and 3D-FEM results to Hashin-Strikman bounds ($\Sigma_m = 0$)

f	Σ_{eqv}^{Gurson}	Σ_{gps}^{stat}	Σ_{gps}^{kine}	H-S bound
0.01	1.71473	1.70501	1.70832	1.70904
0.1	1.55885	1.51393	1.52016	1.50935
0.2	1.38564	1.33165	1.34035	1.30158
0.3	1.21244	1.16114	1.17101	1.10680
0.4	1.03923	0.98765	1.00029	0.92338
0.5	0.86602	0.80637	0.82311	0.75

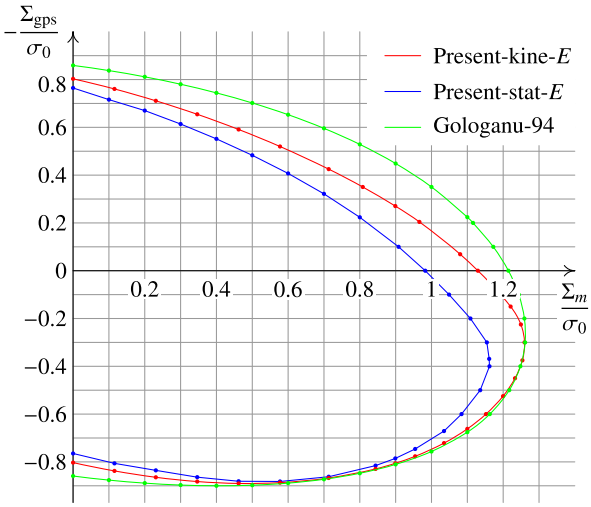

Fig. 4 Comparison of the 1994-Gologanu criterion with numerical bounds. The aspect ratio is taken as $a_1/b_1 = 0.2$ and the porosity f equal to 0.1

than the present static value, 1.5139. This static bound is obtained by using a mesh of 13 layers of 12×12 triangles generating 26,208 discontinuous linear tetrahedrons, i.e., a very refined 3D-mesh for the discretized one-eighth of sphere. Taking into account the fact that the exact value on the horizontal axis is just situated between the very close static and kinematic values, this should indicate that the hollow sphere model does not strictly account for the randomly porous hypothesis of the H-S bounds. Finally the results of Table 2 confirm this conclusion, since the static results are no longer close to the H-S bounds for greater porosity values.

5.2 Confocal Oblate Cavity, Uniform Strain Rate Loading

In this section we compare our results with the analytic criterion of Gologanu [6] and its improved version in [7], under uniform strain rate at the boundary. Figures 4 and 5 give the present results together with those of Gologanu et al. for $f = 0.1$.

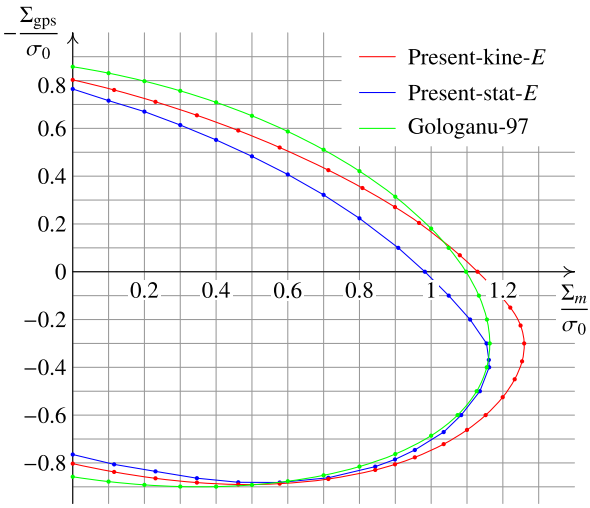

Fig. 5 Comparison of the 1997-Gologanu criterion with numerical bounds. $a_1/b_1 = 0.2$, $f = 0.1$

It first appears that the numerical bounds provide yield surfaces satisfactorily close to each other, in particular for the lowest porosity. Moreover, for this low porosity, the first approximate yield surface given by Gologanu et al. in 1994, based on axisymmetric fields proposed by Lee and Mear [11], is largely beyond our upper bound and overestimates the exact criterion in a large part of the stress domain. *A contrario* the second criterion of Gologanu et al. denotes a significant improvement of the previous Gologanu approach, with a slight localized violation of the numerical static approach possibly due to the loss of the upper bound character, resulting from the approximations done by these authors.

6 Conclusion

In the present paper, we have presented the extension of our previous 3D static and kinematic FEM codes for von Mises matrices to the spheroid (confocal) cavity case. On purpose of validation the first applications concern the Gurson model, and reveal that this criterion is not so near to the real solution, which depends on the third stress invariant in a non-negligible manner. The following tests concern the spheroid confocal cavity case and the last Gologanu criterion should be preferred in the case of uniform strain rate on the boundary.

References

1. Benzerga, A.A., Besson, J.: Plastic potentials for anisotropic porous solids. Eur. J. Mech. A, Solids **20**, 397–434 (2001)
2. Danas, K., Idiart, M.I., Castañeda, P.P.: A homogenization-based constitutive model for isotropic viscoplastic porous media. Int. J. Solids Struct. **45**, 3392–3409 (2008)

3. Francescato, P., Pastor, J., Riveill-Reydet, B.: Ductile failure of cylindrically porous materials. Part i: plane stress problem and experimental results. Eur. J. Mech. A, Solids **23**, 181–190 (2004)
4. Garajeu, M., Suquet, P.: Effective properties of porous ideally plastic or viscoplastic materials containing rigid particles. J. Mech. Phys. Solids **45**, 873–902 (1997)
5. Gologanu, M.: Etude quelques problèmes de rupture ductile des métaux. Thèse de doctorat, Université Paris-6 (1997)
6. Gologanu, M., Leblond, J., Perrin, G., Devaux, J.: Approximate models for ductile metals containing non-spherical voids—case of axisymmetric oblate ellipsoidal cavities. J. Eng. Mater. Technol. **116**, 290–297 (1994)
7. Gologanu, M., Leblond, J., Perrin, G., Devaux, J.: Recent extensions of gurson's model for porous ductile metals. In: Suquet, P. (ed.) Continuum Micromechanics. Springer, Berlin (1997)
8. Gurson, A.L.: Continuum theory of ductile rupture by void nucleation and growth—part I: yield criteria and flow rules for porous ductile media. J. Eng. Mater. Technol. **99**, 2–15 (1977)
9. Kammoun, Z., Pastor, F., Smaoui, H., Pastor, J.: Large static problem in numerical limit analysis: a decomposition approach. Int. J. Numer. Anal. Methods Geomech. **34**, 1960–1980 (2010)
10. Leblond, J.B., Perrin, G., Suquet, P.: Exact results and approximate models for porous viscoplastic solids. Int. J. Plast. **10**, 213–235 (1994)
11. Lee, B., Mear, M.: Axisymmetric deformation of power-law solids containing a dilute concentration of aligned spheroidal voids. J. Mech. Phys. Solids **40**, 1805–1836 (1992)
12. MOSEK ApS: C/O Symbion Science Park, Fruebjergvej 3, Box 16, 2100 Copenhagen ϕ, Denmark (2002)
13. Monchiet, V., Cazacu, O., Charkaluk, E., Kondo, D.: Macroscopic yield criteria for plastic anisotropic materials containing spheroidal voids. Int. J. Plast. **24**, 1158–1189 (2008)
14. Monchiet, V., Charkaluk, E., Kondo, D.: An improvement of Gurson-type models of porous materials by using Eshelby-like trial velocity fields. C. R., Méc. **335**, 32–41 (2007)
15. Pastor, F., Kondo, D., Pastor, J.: Numerical limit analysis bounds for ductile porous media with oblate voids. Mech. Res. Commun. **38**, 250–254 (2011)
16. Pastor, F., Loute, E., Pastor, J.: Limit analysis and convex programming: a decomposition approach of the kinematical mixed method. Int. J. Numer. Methods Eng. **78**, 254–274 (2009)
17. Pastor, J.: Analyse limite: détermination numérique de solutions statiques complètes. Application au talus vertical. J. Méc. Appl. **2**, 167–196 (1978)
18. Pastor, J., Castaneda, P.P.: Yield criteria for porous media in plane strain: second-order estimates versus numerical results. C. R., Méc. **330**, 741–747 (2002)
19. Pastor, J., Francescato, P., Trillat, M., Loute, E., Rousselier, G.: Ductile failure of cylindrically porous materials. part II: other cases of symmetry. Eur. J. Mech. A, Solids **23**, 191–201 (2004)
20. Thai-The, H., Francescato, P., Pastor, J.: Limit analysis of unidirectional porous media. Mech. Res. Commun. **25**, 535–542 (1998)
21. Thoré, P., Pastor, F., Kondo, D., Pastor, J.: Hollow sphere models, conic programming and third stress invariant. Eur. J. Mech., A Solids (2010, in press)
22. Thoré, P., Pastor, F., Pastor, J., Kondo, D.: Closed form solutions for the hollow sphere model with Coulomb and Drucker-Prager materials under isotropic loadings. C. R. Méc., Acad. Sc. Paris **337**, 260–267 (2009)
23. Trillat, M., Pastor, J.: Limit analysis and Gurson's model. Eur. J. Mech. A, Solids **24**, 800–819 (2005)
24. Tvergaard, V.: Influence of voids on shear band instabilities under plane strain conditions. Int. J. Fract. Mech. **17**, 389–407 (1981)
25. Tvergaard, V., Needleman, A.: Analysis of the cup-cone fracture in a round tensile bar. Acta Metall. **32**, 157–169 (1984)